Therapeutic potential of coconut and ginger oils in chronic murine toxoplasmosis

Original Article

Heba M El Naggar[1], Mai A Shehata[1], Hagar F Abdelmaksoud[2], Ashraf M Barakat[3], Reda M Abdelhameed[4], Omnia S Mohammad[1], Ayman M El-Ashkar[1]

Departments of Medical Parasitology[1], Faculty of Medicine, Ain Shams University[1], Cairo, and Theodor Bilharz Research Institute[2], Giza; Zoonotic Diseases, National Research Centre[3], and Applied Organic Chemistry, Chemical Industries Research Institute[4], Giza; Egypt

ABSTRACT

Background: Since current therapies for toxoplasmosis are only effective against tachyzoites in acute infections, and the occurrence of drug resistance, researches are directed to use natural products in the treatment of chronic toxoplasmosis.

Objective: To investigate the potential efficacy of metal-organic framework (MOF) loaded coconut oil (CO) and ginger oil (GO) nanoparticles (NPs) in the treatment of chronic murine toxoplasmosis.

Material and Methods: Ninety laboratory bred Swiss Albino mice were divided into 8 groups (10 mice each); GI (negative control), GII (infected control), GIII-GVIII (infected with Me49 strain of *T. gondii* and treated with MOFs-NPs, Spiramycin, Spiramycin loaded on MOFs-NPs, CO-MOF-NPs, GO-MOF-NPs, and CO+GO-MOFs-NPs, respectively). Parameters used for evaluation included brain cyst count, tissue pathology, and $CD8^+$ infiltration of the liver.

Results: A statistically significant difference was observed in the number of brain cysts between all infected groups receiving treatment, and GII; and GV showed the lowest count of brain cysts with a 60.8% reduction. Histopathological examination showed that loading CO and GO separately or combined with MOFs-NPs significantly restored the normal architecture of all examined tissues, i.e., brain, eye, liver, and kidney. Using immunohistochemical (IHC) staining, high-density $CD8^+$ infiltration was recorded in the liver section of both GI and GII. While GIII, GIV, and GVI displayed low-density $CD8^+$ infiltration, GV, GVII, and GVIII showed intermediate-density.

Conclusion: Loading on MOFs-NPs, CO, and GO offered promising phytotherapy against chronic toxoplasmosis.

Keywords: coconut oil; chronic toxoplasmosis; ginger oil; metal-organic frameworks; nanoparticles; spiramycin.

Received: 1 March, 2024; **Accepted:** 30 April, 2024.

Corresponding Author: Ayman M. El-Ashkar; **Tel.:** +20 1030876995; **Email:** aymanpara@yahoo.com; galaxy202521@gmail.com

Print ISSN: 1687-7942, **Online ISSN:** 2090-2646, **Vol. 17, No. 1, April, 2024.**

INTRODUCTION

The protozoan parasite *T. gondii* is the cause of toxoplasmosis, a very common illness that affects many people globally. There are numerous routes via which this zoonosis is spread, rendering it of great medical and veterinary significance[1]. It is estimated that the parasite infects over two billion people worldwide. The prevalence of the illness varies depending on location, weather, dietary habits, past cat ownership, levels of education, and sanitation standards. Contaminated food or water is the main cause of human infection[2,3].

Although toxoplasmosis typically causes only mild illness in healthy individuals, it poses a significant risk of death to immunocompromised patients due to reactivation in the CNS[4]. Nearly 30% of people have toxoplasmosis, which can be fatal for immunocompromised individuals. The most associated condition with toxoplasmosis is HIV/AIDS[5].

For years, there has been hardly any change in the treatment of individuals with toxoplasmosis. For treatment of symptomatic toxoplasmosis, prescribed combinations of pyrimethamine and sulfadiazine in addition to folinic acid, or pyrimethamine with lincosamide or macrolide antimicrobial agents, are prescribed. Despite significant side effects, the folate pathway-targeting combination therapy of pyrimethamine and sulphadiazine is still the gold standard for treating acute toxoplasmosis[5,6]. Pregnant women typically receive Spiramycin medication to prevent the spread of *T. gondii* through the placenta. While Spiramycin is safe for the treatment of infected mothers, it is ineffective in treating infected children. The prescribed medications prevent *T. gondii* from replicating, but there may be several serious side effects. Spiramycin has a low blood-brain barrier penetration efficacy and low bioavailability. Therefore, a combination of pyrimethamine and sulphadiazine, clindamycin and atovaquone, or clindamycin and pyrimethamine is

 DOI: 10.21608/puj.2024.273767.1239

used to treat *Toxoplasma* encephalitis. When these drug combinations are used over extended periods, serious side effects may occur[7]. Furthermore, it was demonstrated that ciprofloxacin was effective against acute toxoplasmosis and that loading it on silver nanoparticles increased its efficiency[8]. However, it has been demonstrated that ciprofloxacin increases the risk of foetal malformations, abortion, and preterm infants[9,10]. Furthermore, medications do not affect the parasite's tissue cysts, which are mostly found in the muscles and brain. Therefore, it is imperative to create new medications and "gold standard" treatments[6].

Coconut palm plantations was used for centuries in African nations as a natural medicinal therapy. Using a coconut leaf extract, amyloid-β1–42 aggregation and paralysis were decreased in *C. elegans*[11]. Leaf extract of coconut plant was reported to have antiparasitic activity against *P. falciparum*[12]. It was demonstrated that CO significantly inhibits *Cryptosporidium* spp., and it may also be able to decrease the frequency of oncogenic changes in chronic cryptosporidiosis[13,14].

Zingiberaceae is a perpetual herb that includes *Z. officinale*, a strong aromatic spice used worldwide[15,16]. Considerable anti-helminthic actions were recorded against *H. nana*[17], hydatid cysts either *in vitro* or *in vivo*[18], and *T. canis*[19]. Besides, it exhibits an anti-protozoal impact on *T. brucei brucei*[20], *G. lamblia*[21], *Blastocystis* spp.[22], and *Babesia*[23].

Nanoparticles (NPs) are categorized differently depending on their traits, forms, or dimensions; among them are metal, ceramic, and polymeric. Due to their minute size, vast surface area, and unique structure, NPs have special physical and chemical characteristics suitable for a range of domestic and commercial applications[24]. On the other hand, MOFs are a subclass of remarkably porous substances in which the metal or organic linker can be easily changed to modify the drug-loading potential[25]. It was reported that MOFs were utilized as therapeutic agents against bacteria, systems for administering drugs, pharmaceutical substances, phototherapies, nanozymes, and the creation of sensors for assays that identify certain infections[26]. A novel, experimental structure known as nano-curcumin@MOFs was utilized for the treatment of chronic infection with *T. gondii*[27].

In light of the prior layout, this study evaluated the efficacy of CO and GO loaded MOFs-NPs for the treatment of mice with chronic toxoplasmosis using parasitological, histopathological, and IHC parameters.

MATERIAL AND METHODS

This experimental case-control study was conducted at the National Research Centre (NRC) during the period from December 2022 to December 2023.

Study design: Mice were infected with Me49 non-virulent strain of *T. gondii*. At 8 wpi, different animal groups were treated with MOFs-NPs, Spiramycin, Spiramycin loaded MOFs-NPs, CO loaded MOFs-NPs, GO loaded MOFs-NPs, and CO combined with GO loaded MOFs-NPs. Parasitological, histopathological, and immunohistochemical studies were performed.

Animals: The NRC's animal house was the source for 90 male laboratory bred Swiss albino mice. When the mice were 45 d, i.e., 20-25 gm, every 10 mice were kept in a plastic cage. The cages were provided with the following accommodation conditions: white wood chips for bedding; a commercial complete food mixture; tap water; 12 h light alternate with 12 h dark; and temperature of 25±2°C. The stools of the mice under study were examined to exclude any parasitic infection[28].

Animal groups: Table (1) describes the study groups.

Parasite and experimental infection: Every eight weeks, mice in the study were given 0.1 ml of ground homogenous brain tissue having approximately 10 cysts from formerly infected mice through a gastric tube. This was performed to repeatedly maintain the Me49 non-virulent strain of *T. gondii* and cause chronic toxoplasmosis. Cerebral tissues of mice brains were pulverized by a sterile pestle and mortars, and the resulting suspension of cerebral cysts was obtained by diluting the mixture with saline to a concentration of

Table 1. Study groups.

Group number (10 mice each)	Infection status	Treatment		
		Drug	Dose	Reference
GI	Not infected	Not treated		
GII	Infected	Not treated		
GIII	Infected	MOFs-NPs *	100 mg/kg/day	[29]
GIV	Infected	Spiramycin *	100 mg/kg/ day	[30]
GV	Infected	Spiramycin loaded MOFs-NPs (SL-MOFs-NPs) *	A	
GVI	Infected	CO-loaded MOFs-NPs *	0.2 mg/kg/day	[14]
GVII	Infected	GO-loaded MOFs-NPs *	20 mg/kg/day	[31]
GVIII	Infected	CO + GO-loaded MOFs-NPs *	B	

GI: Negative control; **GII:** Positive control; **GIII-GVIII:** Infected, treated with (GIII: MOF-NPs; GIV: Spiramycin; GV: SL-MOFs-NPs; GVI: CO-MOF-NPs; GVII: GO-MOFs-NPs; GVIII: CO+GO-MOF-NPs); ***:** The beginning of drug administration was at 8 wpi for 2 w by gavage using an oesophageal tube[32]; **A:** GV gets the same dose as GIV and GIII; **B:** GVIII gets the same doses as GVI and GVII.

100 cysts/ml by a hemocytometer[33]. The discovery of *T. gondii* brain cysts in a Giemsa-stained cerebral tissue homogenate two months after infection proved that infection was established.

Spiramycin® (Spirex 3 M.I.U): It was purchased from Medical Union Pharmaceuticals as film-coated tablets. The tablets were ground, and the daily dosage of Spiramycin for each mouse was determined to be 100 mg/kg. The tablets were then diluted in 100 µl of saline and administered orally for two w, beginning at 8 wpi[30].

Preparation of CO and GO: We bought mature coconuts (*Cocos nucifera* L.) from a store in the Egyptian province of Giza. To obtain a concentrated water extract, coconuts were dehusked and cracked manually. The extract was then precisely filtered using a membrane filter and then concentrated by a rotary evaporator (Rotatory evaporator, Buchi, Switzerland) with pressure application[14]. We bought dried *Z. officinale* rhizomes from a nearby herbal store in Cairo, Egypt. For the extraction procedure, the plant samples were pulverized in an electric mill to a fine powder. The plant extraction procedure: 500 gm of dried *Z. officinale* were steeped in 85% methanol for a week, filtered many times through Whatman No. 1 filter paper, and then concentrated using a Buchi rotatory evaporator at 4000C to eliminate all methanol[31].

Preparation of NH2-MIL-125 NPs: To create NH2-MIL-125, 1 ml (3.38 mmol) of titanium isopropoxide and 1 g (5.5 mmol) of 2-amino terephthalic acid were dissolved in a room-temperature combination of dimethylformamide (DMF) and methanol (2:1 v/v). After obtaining the slurry, it was sealed and baked for 20 h at 150°C. Eventually, a pale yellow substance was acquired. After filtering off the product and washing it with DMF to get rid of the organic ligand that hadn't reacted, it was rinsed with methanol once more to replace DMF[34,35].

Drug loading: To load the medication onto NH2-MIL-125 nanoparticles, 100 ml of ethanol was used to dissolve coconut and ginger at various concentrations (100–1000 ppm). A magnetic stirrer set at 600 rpm was used to mix medication solutions containing 1 g of NH2-MIL-125 nanoparticles for 90 min at room temperature. The solution was left for the entire night, then centrifuged for five minutes at 5,000 rpm. The precipitate and supernatant were separated. By comparing the concentration of ginger and coconut in the solution before and after drug loading, the amount of loaded drug was ascertained. The following formula was used to determine the proportion of medication loading: Drug loading percentage = [(A-B)/A] ×100, where A and B stand for the start and end drug concentrations of the drug solution[36,37].

Characterization of MOFs: X-ray diffraction (XRD) patterns were performed to demonstrate the phase purity and crystallinity of the produced materials (using an X'Pert MPD Philips diffractometer; Cu Kα was the monochromated material). Using a transmission electron microscope and a scanning electron microscope (SEM: Hitachi SU-70, JP), the nanostructure morphology of MOFs was examined[38].

Parasitological examination: After 10 wpi, the scarification of all mice was done by euthanasia using the behead technique[39]. Every removed brain was split lengthwise into 2 parts. One of the 2 parts was preserved in 10% formalin for histological analysis followed by staining with haematoxylin and eosin (H&E) and the other was used for parasitological counting of brain cysts. The latter was homogenized in sterile saline solution. Subsequently, 50 ul of cerebral tissue homogenate was allowed to air dry, fixed with methanol, stained for 30 min with 10% Giemsa stain, washed with water, and left to dry at room temperature. Coverslips were affixed using a DPX mounting solution. Ultimately, the cysts were counted using a compound microscope. The total count of cysts in every brain was calculated, and the mean for different groups was estimated[40,41]. Count of cerebral cysts/ml = Number of cysts in 50 ul (0.05 ml)/0.05. Count of cerebral cysts in the entire brain = cysts /ml x volume of brain homogenate x 2.

Histopathological examination: At 10 wpi, all animals were sacrificed, and the cerebral, ocular, hepatic, and renal tissue were excised and kept in a 10% buffered formalin solution before being sectioned. In the NRC pathology laboratory, sectioned paraffin wax blocks were used for tissue embedding, and the pathological alterations and effects of different drugs on the infected animals were assessed by staining them with H&E[42].

Immunohistochemical examination: Paraffin slices were applied on positively charged slides using the avidin-biotin-peroxidase complex (ABC) method. After sections from each group were subjected to mouse $CD4^+$ monoclonal antibody (Elabscience, Cat# E-AB-22098, Dil.: 1:100) and mouse $CD8^+$ monoclonal antibody (Elabscience, Cat# PA5036, Dil.: 1:50), the reagents needed for the ABC technique were added (Vectastain ABC-HRP kit, Vector laboratories). Markers were produced, labelled, and colored with peroxidase, and diaminobenzidine (DAB, Sigma), respectively to identify antigen-antibody complexes. As a negative control, non-immune serum was utilized rather than primary or secondary antibodies. Slices stained with IHC were examined by an Olympus microscope (BX-53)[43,44].

Statistical analysis: Data analysis was performed by ANOVA and the Post hoc Tukey test. The significance was considered if $P<0.05$.

Ethical consideration: The experiment was carried out in compliance with the NRC's Animal Research Committee institutional norms, using protocol authorization number 147910221.

RESULTS

Characterization of MOFs-NPs: NH2-MIL-125 is a yellow powder, that shows peaks at 6.7, 9.7, 11.6, 15.2, 16.6, 17.9, 19.5, 21.5, 22.6, and 25.3 aligned to a great extent with the simulated PXRD patterns of MIL-125 (Fig. 1). The SEM photos of NH2-MIL-125 before and after loading are shown in (Fig. 2). They can be demonstrated through the SEM photos of NH2-MIL-125 before and after loading the dispersed drug on the external surface of NH2-MIL-125. Significantly, there are no nanoparticles visible in NH2-MIL-125 after loading that is different from the initial NH2-MIL-125 material, demonstrating that the insertion of the drug hasn't affected the NH2-MIL-125 morphology and the interaction between the drug and NH2-MIL-125 can be established through chemical bonding.

Drug loading: The competency for drug loading of NH2-MIL-125 was evaluated. It is related to the concentration of the drug and the ratio of NH2-MIL-125 NPs. The drug loading capacity rose with the elevation in these parameters. It rose to reach a plateau at a special value (Fig. 3a). The loading amount in Qm was equal to 271.2 mg/g with 100 ppm drug concentration and stirring at different times. A direct relation between time and drug loading was noted. The greatest drug loading was reported at 90 min (Fig. 3b).

Brain cyst count: Statistically significant differences were recorded (P<0.001) between the different infected treated groups and GII. The lowest number of cerebral cysts was noted in GV (infected, treated with SL-MOFs-NPs) with a statistically significant difference (P<0.001) from other study groups. GIV is second to GV with a reduction of brain cyst count by (56.4%) followed by GVI, GVIII, GVII, and lastly GIII respectively (Table 2).

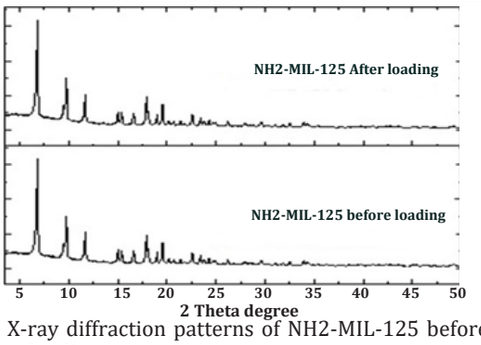

Fig. 1. X-ray diffraction patterns of NH2-MIL-125 before and after loading.

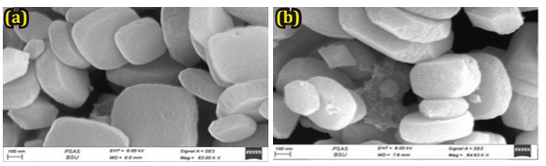

Fig. 2. Micrographs for NH2-MIL-125; **(a)** before loading with the drug, **(b)** after loading with the drug.

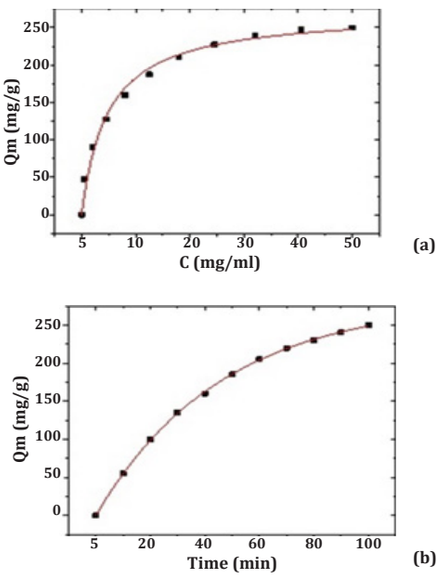

Fig. 3. The balance between the various drug concentrations and the loading dose **(a)**. Impact of contact time **(b)**.

Table 2. Differentiation between the animal groups for the count of brain cysts.

Animal group (n=10)	Brain cysts count Mean±SD	Reduction %	Statistical analysis@
GII	738.5 ± 31.86		
GIII	461.9 ± 24.04[a]	26.8%	
GIV	322.3 ± 14.11[ab]	56.4%	
GV	289.7 ± 11.63[abc]	60.8%	F = 633.3
GVI	325.2 ± 11.00[abd]	56.0%	P <0.001*
GVII	540.3 ± 20.34[abcde]	37.5%	
GVIII	389.1 ± 18.30[abcdef]	47.3%	

GII: Positive control; **GIII-GVIII:** Infected, treated with (GIII: MOF-NPs; GIV: Spiramycin; GV: SL-MOFs-NPs; GVI: CO-MOF-NPs; GVII: GO-MOFs-NPs; GVIII: CO+GO-MOF-NPs); **a:** Significant versus GII, **b:** Significant versus GIII, **c:** Significant versus GIV, **d:** Significant versus GV, **e:** Significant versus GVI, **f:** Significant versus GVII. **@:** ANOVA test with post-hoc Tukey HSD test. ***F*:** F value of ANOVA test, ***:** Significant (P<0.001).

Histopathological examination

Brain sections: GI showed normal architecture of the brain (Fig. 4A). GII, GIII, GIV, GV, and GVII showed necrosis in the neurons with vacuolar degeneration in the cytoplasm and pyknosis of nuclei (Fig. 4B, 4C, 4D, 4E1,2, and 4G) respectively. Axonal degeneration was noted in GIII, and GVII, focal gliosis in GIV, and prevascular edema in GV. GVI showed nearly normal appearance of brain tissue, except for mild apoptosis, and nuclear pyknosis (Fig. 4F). GVIII showed nearly normal appearance of cerebral tissue, except for few vacuoles in the cytoplasm, mild apoptosis in few cells, and pyknosis of nuclei (Fig. 4H).

Eye sections: GI displayed normal architecture of the ocular tissue (Fig. 5A), and GII-GVIII displayed the disruption of photoreceptor cells and the invasion of mononuclear inflammatory cells into the vitreous (Fig. 5B-5H). The pathologic picture was more prominent in GII and milder in the other study groups.

Liver sections: GI showed normal liver tissue structure (Fig. 6A). GII showed eosinophilic cytoplasm, necrotic regions linked to focal invasion of mononuclear cells, profoundly pyknotic nuclei with dilated blood sinusoids, and slight Kupffer cell reactivity (Fig. 6B). GIII showed minimal degenerations and Kupffer cell activation, with sinusoidal enlargement (Fig. 6C). GIV displayed pyknotic nuclei, degeneration, minor necrosis, inflammatory cell invasion, sinusoidal expansion, and mild Kupffer cell reactivity (Fig. 6D). GV revealed hepatocytes with pyknosis of their nuclei and localized infiltration of mononuclear inflammatory cells between them (Fig. 6E). GVI and GVII showed ameliorative effects with sinusoids expansion, and minimal Kupffer cells activity (Fig. 6F, G). GVIII showed more or less similar to normal architecture with few changes like necrosis, sinusoidal expansion, and mild Kupffer cell activity with nuclei pyknosis (Fig. 6H).

Kidney sections: GI displayed a picture of normal kidney tissue (Fig. 7A). GII, GIII, and GV revealed localized invasion of mononuclear inflammatory cells among the renal tubules (Fig. 7B, C, E). In addition, GII displayed an enlargement of urinary space and congested peritubular blood vessels (Fig. 7B), GIII and GVI displayed necrosis in many renal tubules with nuclear pyknosis in the epithelium of the renal tubules (Fig. 7C, F), GIV showed degeneration, pyknosis in the epithelium of renal tubules (Fig. 7D), GV revealed an enlargement of urinary space and congested peritubular blood vessels with nuclear pyknosis in the epithelium of the renal tubules (Fig. 7E), GVII as well as GVIII revealed improvement of renal tissue pathology with minimal necrosis and nuclear pyknosis of the renal tubular epithelium (Fig. 7G, H).

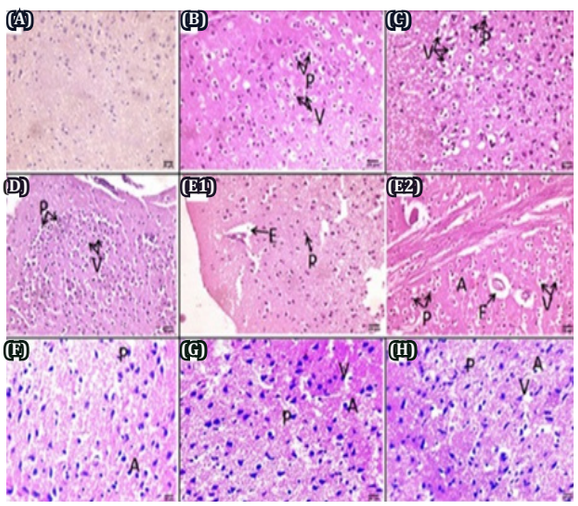

Fig. 4. Histopathologic examination (H&E) of brain sections from different groups. **(A):** GI shows normal architecture of the cerebral tissue; **(B):** GII shows necrosis in the neurons with vacuolar degeneration in the cytoplasm **(V)** and pyknosis of nuclei **(P)**; **(C):** GIII shows necrosis in the neurons with vacuolar degeneration in the cytoplasm **(V)** and pyknosis of nuclei **(P)** with evident degeneration of neuronal axons **(A)**; **(D):** GIV shows focal gliosis **(G)** and necrosis in the neurons with vacuolar degeneration in the cytoplasm **(V)** and pyknosis of nuclei **(P)**; **(E1 and E2):** GV shows necrosis in the neurons with vacuolar degeneration in the cytoplasm **(V)** and pyknosis of nuclei **(P)** with evident prevascular edema **(E)**; **(F):** GVI shows a nearly normal appearance of brain tissue, except for a few apoptosis **(A)**, and nuclear pyknosis **(P)**; **(G):** GVII shows necrosis in the neurons with vacuolar degeneration in the cytoplasm **(V)** and pyknosis of nuclei **(P)** with evident degeneration of neuronal axons **(A)**; **(H):** GVIII shows a nearly normal appearance of cerebral tissue, except for mild vacuolation in the cytoplasm **(V)**, few apoptosis of neuronal axons **(A)**, and nuclear pyknosis **(P)**. **(A-H: X100)**.

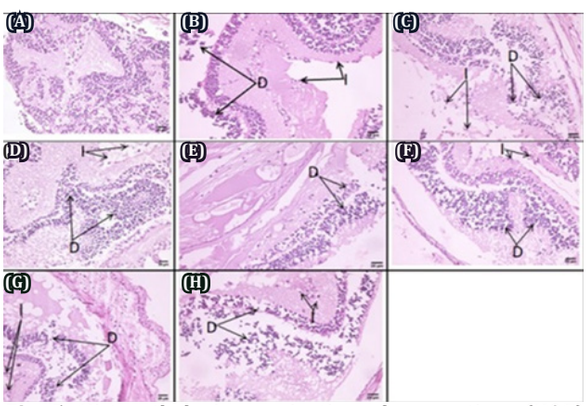

Fig. 5. Histopathologic examination of eye sections (H&E) from different groups. **(A):** GI shows normal architecture of the eye tissue; **(B):** GII shows severe disruption of photoreceptor cells **(D)** and the invasion of mononuclear inflammatory cells into the vitreous **(I)**; **(C-H):** GIII-GVIII show milder disruption of photoreceptor cells **(D)** and the invasion of mononuclear inflammatory cells into the vitreous **(I)**. **(A-E and G: X40, F and H: X100)**.

Immunohistochemical examination of liver tissues: High-density $CD8^+$ infiltration was noted in GI and GII, intermediate-density in GV and GVII, and low-density $CD8^+$ infiltration in GIII, GIV, and GVI (Fig. 8 A-H).

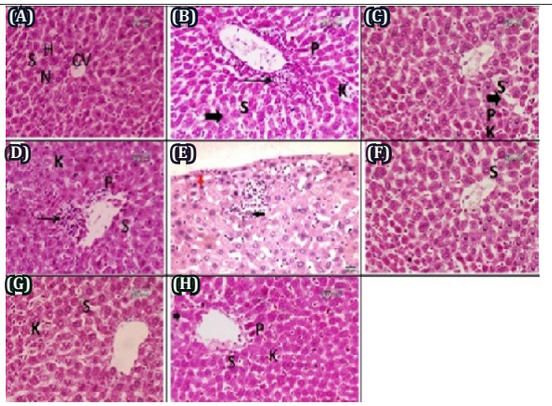

Fig. 6. Histopathologic examination of liver sections (H&E) from different groups. **(A):** GI shows normal liver tissue structure; **(B):** GII shows eosinophilic cytoplasm, necrotic regions (arrowhead) linked to focal invasion of mononuclear cells (arrow), profoundly pyknotic nuclei with dilated blood sinusoids **(S)**, and slight Kupffer cell reactivity **(K)**; **(C):** GIII shows minimal degenerations and Kupffer cell activation **(K)**, with sinusoidal enlargement **(S)**; **(D):** GIV displays nuclear pyknosis **(P)**, degeneration, minor necrosis (arrowhead), inflammatory cell invasion, sinusoidal expansion, and mild Kupffer cell reactivity **(K)**; **(E):** GV reveals hepatocytes with pyknosis of their nuclei (red arrow) and local invasion of mononuclear inflammatory cells between them (black arrow); **(F,G)**: GVI and GVII show remarkable improvement with sinusoid expansion **(S)**, and minimal Kupffer cells activity **(K)**; **(H):** GVIII show more or less similar to normal architecture with few changes like necrosis (arrowhead), sinusoidal expansion, and mild Kupffer cell activity **(K)** with nuclei pyknosis **(P)**. **(A-H: X100)**.

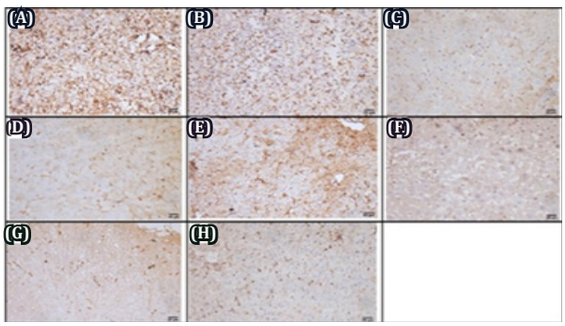

Fig. 8. IHC results for liver sections of different study groups (IHC- peroxidase-DAB). High-density $CD8^+$ infiltration was noted in GI and GII, intermediate-density in GV and GVII and low-density in GIII, GIV, and GVI. **(A-H: X400)**.

DISCUSSION

Drugs currently used for the treatment of toxoplasmosis either have several negative adverse reactions or are useless when the disease is in its chronic stage[45]. In the present study, CO and GO were used against murine toxoplasmosis. Medicinal plants were successfully examined against coccidian parasites. Coconut oil[13,14], *Verbena officinalis*[46], wheat germ oil[47,48], and Asafoetida[49] were successfully investigated against *C. parvum*. Several studies reported

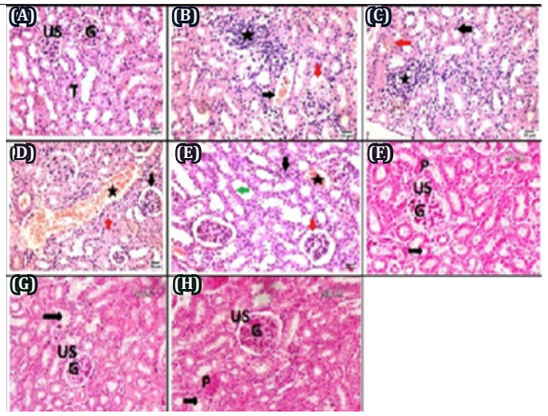

Fig. 7. Histopathologic examination of kidney sections (H&E) from different groups. **(A):** GI shows normal architecture of the renal tissue with glomerulus **(G)**, urinary space **(US)**, and tubules **(T)**; **(B):** GII shows localized invasion of mononuclear inflammatory cells among the renal tubules (star), enlargement of urinary space (red arrow), and congested peritubular blood vessels (black arrow); **(C):** GIII shows localized invasion of mononuclear inflammatory cells among the renal tubules (star) necrosis in the epithelium of many renal tubules (red arrow) with nuclear pyknosis (black arrow); **(D):** GIV shows degeneration (arrowhead), and pyknosis **(P)** in the epithelium of renal tubules; **(E):** GV shows localized invasion of mononuclear inflammatory cells among the renal tubules (black arrow), enlargement of urinary space (red arrow), and congested peritubular blood vessels (star) with nuclear pyknosis (green arrow) in the epithelium of the renal tubule; **(F):** GVI shows necrosis and nuclear pyknosis in the epithelium of the renal tubules; **(G,H):** GVII, and GVIII show improvement of renal tissue pathology with minimal necrosis (arrowhead) and nuclear pyknosis **(P)** of the renal tubular epithelium. **(A-H: H&E X100)**.

that various botanical extracts revealed therapeutic activities against toxoplasmosis like *N. sativa*[32], *Z. officinale*[50], and *F. asafetida*[51].

In this study, the antiparasitic effects of various drugs and medicinal plants were evaluated by quantifying cerebral cysts of *T. gondii*. Our results are consistent with a study that revealed a considerable ability of *T. gondii* to infect the brains of man and other vertebrates with the establishment of latent infection[52]. There were statistically significant variations (P<0.001) regarding the number of cerebral cysts between the infected groups that received different remedies and the positive control group. Moreover, GV revealed the lowest number of cerebral cysts with a significant difference (P<0.001) from other groups with a 60.8% reduction compared to GIII (positive control). Group IV is second to GV with reduction of brain cyst count by (56.4%) followed by groups GVI, GVIII, GVII, and lastly GIII in which the percentages of reduction of brain cysts were 56%, 47.3%, 37.5%, and 26.8%, respectively. Our results are also comparable with El Naggar *et al*.[53] who recorded the highest percentage of cerebral cyst reduction (53.6%) in GV (infected treated

with honeybee venom (BV)-MOF-NPs, followed by the infected groups treated with [GVIII (Ciprofloxacin alone), GIX (ciprofloxacin- MOF-NPs), GVII (Spiramycin-MOF-NPs), GIV (BV alone), GVI (Spiramycin-MOFs-NPs) and lastly GIII (MOF-NPs alone)] in which the percentages of reduction of brain cysts were (50.4%, 50%, 49.6%, 49%, 48.5%, and 22.8%), respectively. EL-Ashkar *et al*.[54] found that the group treated with Spiramycin-metronidazole had fewer brain cysts compared to the infected control group.

Moreover, this aligns with Mohammad *et al*.[32] who found statistically significant differences (P<0.001) between the study groups and the positive control group. The study groups receiving *N. sativa* oil (NSO) treatment after loading on copper-benzene tricarboxylic acid metal-organic frameworks (NSO@ Cu-BTC MOF) had the lowest brain cyst count. This group was followed by a group treated with a combination of NSO and wheat germ oil (WGO) loaded on Cu-BTC MOF (WGO+NSO@Cu-BTC MOF) and then WGO@Cu-BTC MOF, which resulted in a significant decrease in the burden of cerebral cysts (64.3%, 51.4%, and 49.5%, respectively). Moderate percentages of the decline of cerebral cyst count were noted in the groups that received Spiramycin separately and after loading on Cu-BTC-MOF (42.4%, 41.8%, respectively). The group that received Cu-BTC-MOF alone showed the least reduction percentage (24.4%) among the infected groups. Our study followed the same time regimen for drug application in addition to the scarification of animals. Infection was established by the ME49 strain of *T. gondii,* then treatment by Spiramycin separately and after loading on Cu-BTC MOF in a dose of 200 mg/kg body weight/day that is double the dose used to treat GIV and GV in this experiment. This may indicate more efficiency of NH2-MIL-125 when loaded with Spiramycin than Cu- BTC MOF. This aligns also with Karimi *et al*.[55] who proved the lethal impact of ginger extract-based silver NPs on *T. gondii* and their induction of apoptosis. Our results could be supported by El-Kady *et al*.[50] who showed that administering ginger extract to *T. gondii*-infected mice brains dramatically decreased the number of cysts present, markedly reduced oedema and inflammation, and reversed neuronal damage. Additionally, the administration of ginger extract lowered lung and liver inflammation and shielded hepatocytes from infection-related deterioration.

In our experiment, testing the cerebral, hepatic, renal, and eye tissues of mice with chronic toxoplasmosis showed evident effect of CO and GO when loaded alone on MOFs-NPs or in combination. They notably decreased fibrous tissue accumulation, tissue damage, and inflammatory responses. Ginger was proved to have protective properties for the liver, a stimulatory effect on the immune system with cytotoxic activities, a defensive impact against oxidative stress, with antagonizing effects against oncogenic and inflammatory processes[56]. This is in congruence with a study demonstrating the coconut palm's (*C. nucifera*) significant alleviation of the inflammatory response[57]. When CO was previously tested in immunosuppressed chronically infected mice with cryptosporidiosis, the pathological changes were dramatically improved with the preservation of the intestinal villous pattern. The CO-treated group also showed very mild villous core inflammation, which appeared to be greater than the healing effect of nitazoxanide[13].

Furthermore, IHC assessment of hepatic tissue showed high-density $CD8^+$ infiltration in GI and GII. The same pattern of infiltration was also noted near the *T. gondii* cerebral cysts[53,58]. Many studies highlighted the significance of $CD8^+$ T-cells in combating *Toxoplasma* cyst formation in different issues[59]. It is worth mentioning that maintaining the function of $CD8^+$ T-cells is crucial for reducing the chronic prevalence of parasites[60]. Moreover, GIII showed low-density $CD8^+$ T-cell infiltration. This aligns with El Naggar *et al*.[53] who reported a low density of $CD8^+$ T-cells when MOF-NPs were used alone. This may elucidate the poor activity of MOF-NPs as an immunostimulant. Besides, GIV as well as GV showed low and intermediate-density $CD8^+$ infiltration. This aligned with Almurshidi *et al*[51] who recorded a reduction of both $CD4^+$ and $CD8^+$ T-cells in the cerebral tissues of chronically infected mice treated with a combination of Spiramycin and *Ferula asafetida*. GVII and GVIII showed intermediate expression while GVI showed low expression of $CD8^+$ T-cells. These results are supported by a study that proved the immunostimulant activity of ginger[64]. Also, CO was recorded to stimulate cytotoxic responses[61].

In conclusion, CO and GO are promising phytotherapies against chronic toxoplasmosis. When loaded on MOF-NPs, they exhibit significant effects against chronic murine toxoplasmosis in the form of reduction of tissue cysts numbers, and improvement of tissue inflammation, degeneration, and fibrosis. Future studies are recommended to identify their optimum dose, and mechanism of action.

Acknowledgment: The authors express their gratitude to Dr. Islam Elgohary, Department of Pathology, Agricultural Research Center, Animal Health Research Institute, Eldokki, Giza, Egypt, for performing the histopathologic examination of the animal tissues.

Author contributions: El Naggar HM, Shehata MA, Abdelmaksoud HF, Mohammad OS, and El-Ashkar AM contributed in the study design, assessment of the parasitological parameters and data analysis. Abdelhameed RM performed the IHC study. Barakat AM supervised the animal accommodation conditions, and their scheduled sacrifice, as well as maintenance of *T. gondii* Me49 strain. All authors revised and accepted the manuscript before publication, and asserted the authorship order.

Conflict of Interest: None.

Funding statement: None.

REFERENCES

1. Attias M, Teixeira D, Benchimol M, Vommaro R, Crepaldi P, De Souza W. The life-cycle of *Toxoplasma gondii* reviewed using animations. Parasit Vectors 2020; 13:1-13.
2. Dubey JP. The history and life cycle of *Toxoplasma gondii*. In: *Toxoplasma gondii*. Academic Press, Bronx, New York, USA, 2nd edition, 2014:1-17.
3. Almeria S, Dubey JP. Foodborne transmission of *Toxoplasma gondii* infection in the last decade: An overview. Res Vet Sci 2021; 135:371-385.
4. Matta S, Rinkenberger N, Dunay I, Sibley L. *Toxoplasma gondii* infection and its implications within the central nervous system. Nat Rev Microbiol 2021; 19:467–480.
5. Shammaa A, Powell T, Benmerzouga I. Adverse outcomes associated with the treatment of *Toxoplasma* infections. Sci Rep 2021; 11.
6. Antczak M, Dzitko K, Długońska H. Human toxoplasmosis: Searching for novel chemotherapeutics. Biomed Pharmacother 2016; 82:677–684.
7. Wei H, Wei S, Lindsay D, Peng H. A systematic review and meta-analysis of the efficacy of anti-*Toxoplasma gondii* medicines in humans. PLoS One 2015; 10:1–12.
8. Ahmed F, Rashed S, Abououf E, Eraky M, Barakat A, Sadek S, *et al*. Effects of Ciprofloxacin loaded on silver nanoparticles on murine acute toxoplasmosis. BMFJ 2022;39(3):941-953.
9. Ziv A, Masarwa R, Perlman A, Ziv D, Matok I. Pregnancy outcomes following exposure to quinolone antibiotics: A systematic review and meta-analysis. Pharm Res 2018; 35.
10. Acar S, Keskin-Arslan E, Erol-Coskun H, Kaya-Temiz T, Kaplan Y. Pregnancy outcomes following quinolone and fluoroquinolone exposure during pregnancy: A systematic review and meta-analysis. Reprod Toxicol 2019; 85:65–74.
11. Manalo RV, Silvestre MA, Barbosa ALA, Medina PM. Coconut (*Cocos nucifera*) ethanolic leaf extract reduces amyloid-β (1-42) aggregation and paralysis prevalence in transgenic *Caenorhabditis elegans* independently of free radical scavenging and acetylcholinesterase inhibition. Biomedicines 2017; 5(2):17.
12. Tayler NM, Boya CA, Herrera L, Moy J, Ng M, Pineda L, *et al*. Analysis of the antiparasitic and anticancer activity of the coconut palm (*Cocos nucifera* L. Arecaceae) from the natural reserve of Punta Patiño, Darién. PLoS One. 2019; 14(4):e0214193.
13. Abdelmaksoud H, Aboushousha T, El-Ashkar A. Efficacy of coconut oil as therapeutic agent with potential anticancer activity in immunosuppressed mice with cryptosporidiosis: Parasitological, histopathological and immunohistochemical studies. PUJ 2022; 15:45–52.
14. El Naggar H, Mohammed B, Aboushousha T, Abdelmaksoud H. Study on the therapeutic effect of coconut oil extracts as an alternative medicinal plant in *Cryptosporidium* infected mice. Turkiye Parazitoloji Dergisi 2023; 47:136–143.
15. Ahmad B, Rehman M, Amin I, Arif A, Rasool S, Bhat S, *et al*. A review on pharmacological properties of zingerone (4-(4-Hydroxy-3-methoxyphenyl)-2-butanone). TSWJ 2015; 2015:1–6.
16. Rahmani A, Al Shabrmi F, Aly S. Active ingredients of ginger as potential candidates in the prevention and treatment of diseases via modulation of biological activities. Int J Physiol Pathophysiol Pharmacol 2014;6(2):125-136.
17. Lin R, Chen C, Lu C, Ma Y, Chung L, Wang J, *et al*. Anthelmintic constituents from ginger (*Zingiber officinale*) against *Hymenolepis nana*. Acta Trop 2014; 140:50–60.
18. Nihad Baqer N, Khuder M, Amer N. Antiprotoscolices effects of ethanolic extract of *Zingiber officinale* against *Echinococcus granulosus in vitro* and *in vivo*. IJAR 2014;2(10):59-68.
19. El-Sayed N. Efficacy of *Zingiber officinale* ethanol extract on the viability, embryogenesis and infectivity of *Toxocara canis* eggs. J Parasit Dis 2017; 41:1020–1027.
20. Kobo P, Erin P, Suleiman M, Aliyu H, Tauheed M, Muftau S, *et al*. Antitrypanosomal effect of methanolic extract of *Zingiber officinale* (ginger) on *Trypanosoma brucei brucei*-infected Wistar mice. Vet World 2014; 7:770–775.
21. Mahmoud A, Attia R, Said S, Ibraheim Z. Ginger and Cinnamon: Can this household remedy treat giardiasis? Parasitological and histopathological Studies. Iran J Parasitol 2014; 9(4):530-540.
22. Abdel-Hafeez EH, Ahmad AK, Kamal AM, Abdellatif MZM, Abdelgelil NH. *In vivo* antiprotozoan effects of garlic (*Allium sativum*) and ginger (*Zingiber officinale*) extracts on experimentally infected mice with *Blastocystis* spp. Parasitol Res 2015; 114:3439–444.
23. Rizk MA, El-Sayed SAE, Igarashi I. Evaluation of the inhibitory effect of *Zingiber officinale* rhizome on *Babesia* and *Theileria* parasites. Parasitol Int 2021;85:102431.
24. Khan I, Saeed K, Khan I. Nanoparticles: Properties, applications and toxicities. Arab J Chem 2019;12:908–931.
25. Trotta F. Metal organic frameworks in medicine. ASPS 2019;3:107–109.
26. Quijia C, Alves R, Hanck-Silva G, Galvão Frem R, Arroyos G, Chorilli M. Metal-organic frameworks for diagnosis and therapy of infectious diseases. Crit Rev Microbiol 2022; 48:161–196.
27. El-Shafey A, Hegab M, Seliem M, Barakat A, Mostafa N, Abdel-Maksoud H, *et al*. Curcumin@metal organic frameworks nano-composite for treatment of chronic toxoplasmosis. J Mater Sci Mater Med 2020; 31(11):90.
28. Garcia L, Bruckner D. Diagnostic Medical Parasitology. 3rd Edition; ASM Press; Washington DC, 1997.
29. Alajmi R, AL-Megrin W, Metwally D, AL-Subaie H, Altamrah N, Barakat A, *et al*. Anti-*Toxoplasma* activity of silver nanoparticles green synthesized with *Phoenix dactylifera* and *Ziziphus spinachristi* extracts which inhibits inflammation through liver regulation of cytokines in Balb/c mice. Biosci Rep 2019; 39(5):BSR20190379
30. Hagras N, Allam A, Farag H, Osman M, Shalaby T, HM F, *et al*. Successful treatment of acute experimental toxoplasmosis by Spiramycin-loaded chitosan nanoparticles. Exp Parasitol 2019; 204:107717.
31. Fawzy E, Sayed Zalat R, Rashed H, Salama M, Saleh A, Fakhry Abdelhamed E. Effect of cinnamon and ginger methanolic extracts on murine intestinal cryptosporidiosis: *In-vivo* evaluation. J Egypt Soc Parasitol 2019; 49(3):689-698.
32. Mohammad O, El Naggar H, Abdelmaksoud H, Barakat A, Abdelhameed R, Shehata M. The effect of *Nigella sativa* oil- and wheat germ oil-loaded metal organic frameworks

on chronic murine toxoplasmosis. Acta Trop 2023; 239:106823.
33. Djurkovic-Djakovic O, Milenković V, Nikolić A, Bobić B, Grujić J. Efficacy of atovaquone combined with clindamycin against murine infection with a cystogenic (Me49) strain of *Toxoplasma gondii*. J Antimicrob Chemother 2002; 50:981–987.
34. Fu Y, Zhang K, Zhang Y, Cong Y, Wang Q. Fabrication of visible-light-active MR/NH2-MIL-125 (Ti) homojunction with boosted photocatalytic performance. Chem En J 2021; 412:128722.
35. Abdelhameed, RM, Tobaldi DM, Karmaoui M. Engineering highly effective and stable nanocomposite photocatalyst based on NH2-MIL-125 encirclement with Ag_3PO_4 nanoparticles. JPPA 2018; 351:50-58.
36. Motakef-Kazemi N, Shojaosadati SA, Morsali A. *In situ* synthesis of a drug-loaded MOF at room temperature. Microporous Mesoporous Mat 2014; 186:73-79.
37. Al Haydar M, Abid HR, Sunderland B, Wang S. Metal organic frameworks as a drug delivery system for flurbiprofen. Drug Des Devel Ther 2017;11:2685-2695.
38. Kim SN, Kim J, Kim HY, Cho HY, Ahn WS. Adsorption/ catalytic properties of MIL-125 and NH2-MIL-125. Catal Today 2013; 204:85-93.
39. Boivin G, Bottomley M, Grobe N. Responses of male C57BL/6N mice to observing the euthanasia of other mice. J Am Assoc Lab Anim Sci 2016; 55:406–411.
40. Chew W, Segarra I, Ambu S, Mak J. Significant reduction of brain cysts caused by *Toxoplasma gondii* after treatment with spiramycin co-administered with metronidazole in a mouse model of chronic toxoplasmosis. Antimicrob Agents Chemother 2012; 56:1762–1768.
41. Etewa S, El-Maaty D, Hamza R, Metwaly A, Sarhan M, Abdel-Rahman S, *et al*. Assessment of spiramycin-loaded chitosan nanoparticles treatment on acute and chronic toxoplasmosis in mice. J Parasit Dis 2018; 42:102–113.
42. Feldman AT, Wolfe D. Tissue processing and hematoxylin and eosin staining. Methods Mol Biol 2014;1180:31–43.
43. Lindsay DS, Dubey JP. Immunohistochemical diagnosis of *Neospora caninum* in tissue section of dogs. Am J Vet Res 1989; 50(11):1981–1983.
44. Dubey JP, Garner MM, Willette MM, Batey KL, Gardiner CH. Disseminated toxoplasmosis in magpie geese (*Anseranas semipalmata*) with large numbers of tissue cysts in livers. J Parasitol 2001;87(1):219–223.
45. Silveira C, Muccioli C, Nussenblatt R, Belfort R. The effect of long-term intermittent trimethoprim/ sulfamethoxazole treatment on recurrences of toxoplasmic retinochoroiditis: 10 years of follow-up. Ocul Immunol Inflamm 2015; 23:246–247.
46. El-Wakil E, El-Shazly M, El-Ashkar A, Aboushousha T, Ghareeb M. Chemical profiling of *Verbena officinalis* and assessment of its anti-cryptosporidial activity in experimentally infected immunocompromised mice. Arab J Chem 2022; 15(7):103945.
47. Abdelmaksoud H, Aboushousha T, El-Ashkar A. Deep glance on the antiparasitic anticancer activities of wheat germ oil in chronically infected immunosuppressed mice with cryptosporidiosis. J Parasit Dis 2022;46(3): 785-794.
48. Abdelmaksoud HF, Osman EEA, Abdel-Hameed SS, Aboushousha T, Naggar HME. *In vivo* evaluation of anticryptosporidial effects of wheat germ extracts in immunocompromised mice. J Parasit Dis 2022; 46(3):833-844.
49. Abdelmaksoud HF, El-Ashkar AM, Elgohary SA, El-Wakil ES. Potential therapeutic and prophylactic effects of *Asafoetida* in murine cryptosporidiosis. J Parasit Dis 2020; 44:646–653.
50. El-Kady A, Al-Megrin W, Abdel-Rahman I, Sayed E, Alshehri E, Wakid M, *et al*. Ginger is a potential therapeutic for chronic toxoplasmosis. Pathogens 2022; 11(7):798.
51. Almurshidi B, Fahmy Z, El-Shennawy A, Selim E, Hammam O, Okasha H, *et al*. A multimodality therapeutic application on *Toxoplasma gondii* encephalitis utilizing Spiramycin and '*de novo*' *Ferula asafetida* in immunodeficient mice. Parasite Immunol 2023; 45(12):e13014.
52. Ross E, Olivera G, Barragan A. Early passage of *Toxoplasma gondii* across the blood–brain barrier. Trends Parasitol 2022; 38:450–461.
53. El Naggar H, Anwar M, Khayyal A, Abdelhameed R, Barakat A, Sadek S, *et al*. Application of honeybee venom loaded nanoparticles for the treatment of chronic toxoplasmosis: Parasitological, histopathological, and immunohistochemical studies. J Parasit Dis 2023; 47(3):591-607.
54. EL-Ashkar A, El-Hosseiny L, Abu Zahra F, Abd El-Samee N, Barakat A, Elgohary S, *et al*. Potential therapeutic effect of allogenic mesenchymal stem cells on chronic cerebral murine toxoplasmosis. AEJI 2020; 10(2):129-140.
55. Saryazdi AKP, Tavakoli P, Barati M, Ghaffarifar F, Dalir Ghaffari A, Saryazdi YKP. Anti-*Toxoplasma* effects of silver nanoparticles based on ginger extract: An *in vitro* study. J Arch Mil Med 2020;7(4):e104248.
56. Bekkouch O, Dalli M, Harnafi M, Touiss I, Mokhtari I, Assri SE, *et al*. Ginger (*Zingiber officinale* Roscoe), lemon (*Citrus limon* L.) juices as preventive agents from chronic liver damage induced by CCl4: A biochemical and histological study. Antioxidants (Basel) 2022;11(2):390.
57. Roopan S. An overview of phytoconstituents, biotechnological applications, and nutritive aspects of coconut (*Cocos nucifera*). Appl Biochem Biotechnol 2016; 179:1309–1324.
58. Etewa S, Al-Hoot A, Abdelmoaty S, Mohammad S, Moawad H, Sarhan M, *et al*. The outcomes of mesenchymal stem cells therapy for experimental toxoplasmosis. PUJ 2019; 12(1):34-44.
59. Landrith T, Harris T, Wilson E. Characteristics and critical function of $CD8^+$ T cells in the *Toxoplasma*-infected brain. Semin Immunopathol 2015; 37:261–270.
60. Khan I, Hwang S, Moretto M. *Toxoplasma gondii*: $CD8^+$ T cells cry for $CD4^+$ help. Front Cell Infect Microbiol 2019; 9:136.
61. Illam S, Narayanankutty A, Mathew S, Valsalakumari R, Jacob R, Raghavamenon A. Epithelial mesenchymal transition in cancer progression: preventive phytochemicals. Recent Pat Anticancer Drug Discov 2017; 12(3): 234-246.